Accepted Manuscript

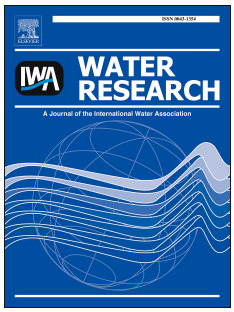

Effects of sulfate on heavy metal release from iron corrosion scales in drinking water distribution system

Huifang Sun, Baoyou Shi, Fan Yang, Dongsheng Wang

PII: S0043-1354(17)30103-3

DOI: 10.1016/j.watres.2017.02.021

Reference: WR 12690

To appear in: *Water Research*

Received Date: 2 November 2016

Revised Date: 8 February 2017

Accepted Date: 10 February 2017

Please cite this article as: Sun, H., Shi, B., Yang, F., Wang, D., Effects of sulfate on heavy metal release from iron corrosion scales in drinking water distribution system, *Water Research* (2017), doi: 10.1016/j.watres.2017.02.021.

Graphic abstract

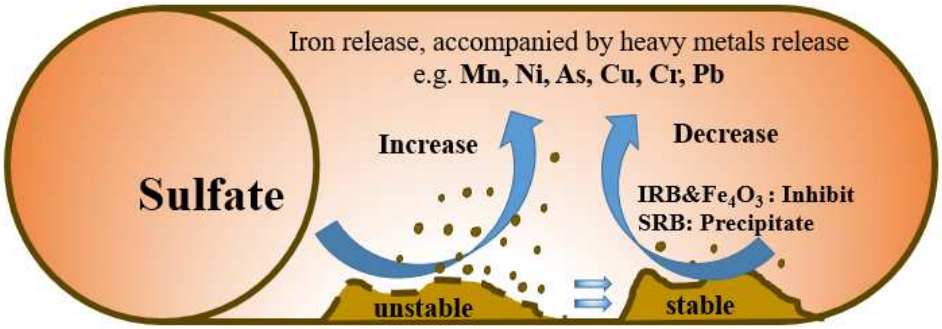

Effects of sulfate on heavy metal release from iron corrosion scales in drinking water distribution system

Huifang Sun[1], Baoyou Shi[2,3*], Fan Yang[4], Dongsheng Wang[2]

[1] Institute of Resources and Environmental Engineering, Shanxi University, Taiyuan, 030006, China

[2] Key Laboratory of Drinking Water Science and Technology, Research Center for Eco-Environmental Sciences, Chinese Academy of Sciences, Beijing, 100085, China

[3] University of Chinese Academy of Sciences, Beijing 100049, China

[4] College of Engineering and Technology, Tianjin Agricultural University, Tianjin 300384, China

*Corresponding author: Tel./Fax: +86 10 62924821.

E-mail address: byshi@rcees.ac.cn

Abstract

Trace heavy metals accumulating in iron corrosion scales within a drinking water distribution system (DWDS) could potentially be released to bulk water and consequently deteriorate the tap water quality. The objective of this study was to identify and evaluate the release of trace heavy metals in DWDS under changing source water conditions. Experimental pipe loops with different iron corrosion scales were set up to simulate the actual DWDS. The effects of sulfate levels on heavy metal release were systemically investigated. Heavy metal releases of Mn, Ni, Cu, Pb, Cr and As could be rapidly triggered by sulfate addition but the releases slowly decreased over time. Heavy metal release was more severe in pipes transporting groundwater (GW) than in pipes transporting surface water (SW). There were strong positive correlations ($R^2 > 0.8$) between the releases of Fe and Mn, Fe and Ni, Fe and Cu, and Fe and Pb. When switching to higher sulfate water, iron corrosion scales in all pipe loops tended to be more stable (especially in pipes transporting GW), with a larger proportion of stable constituents (mainly Fe_3O_4) and fewer unstable compounds (β-FeOOH, γ-FeOOH, $FeCO_3$ and amorphous iron oxides). The main functional iron reducing bacteria (IRB) communities were favorable for the formation of Fe_3O_4. The transformation of corrosion scales and the growth of sulfate reducing bacteria (SRB) accounted for the gradually reduced heavy metal release with time. The higher metal release in pipes transporting GW could be due to increased $Fe_6(OH)_{12}CO_3$ content under the higher sulfate concentrations.

Keywords:

Drinking water distribution system, heavy metal release, iron corrosion scale, sulfate

1. Introduction

The accumulation of heavy metals within drinking water distribution systems (DWDS) has caused considerable concern. Even if heavy metals are present at concentrations below their maximum contaminant levels (MCLs) or at non-detectable levels in treated water, they can accumulate within deposits and corrosion scales that exist in DWDS (Peng *et al.* 2012, Lytle *et al.* 2010, Fisher *et al.* 2000, Lytle *et al.* 2004, Schock *et al.* 2008). Some iron compounds commonly found in corrosion scales, such as goethite (α-FeOOH), lepidocrocite (γ-FeOOH), magnetite (Fe_3O_4) and ferrihydrite have strong affinity to adsorb and concentrate trace heavy metals, such as arsenic (As), chromium (Cr), lead (Pb), vanadium (V) and uranium (U) (Peng *et al.* 2010, Sarin *et al.* 2001). Relative to iron compounds, manganese (Mn) oxides/oxyhydroxides are commonly found in DWDS, and these are highly effective at adsorbing metal ions, such as Cr, copper (Cu), iron (Fe), nickel (Ni), Pb and strontium (Sr) ions (Gerke *et al.* 2016).

The primary concern with trace heavy metals in DWDS is the potential release of the metals back into the water (through particulate transport and/or chemical release, e.g. desorption, dissolution), which may result in elevated heavy metal levels in domestic tap water. For example, there was a major release of lead and other contaminants into a midsized Midwestern distribution system following the introduction of chlorination in the United States. Shortly after chlorination was instituted, numerous colored water complaints were received, and subsequent investigations found high levels of Fe, Cu and As in the colored water specimens (Reiber and Dostal 2000). Lytle *et al.* (2010)

reported As concentration in domestic water was as high as 299 μg L^{-1}, which was nearly six times the MCL of 50 μg L^{-1}. Therefore, drinking water providers should be aware of the potential release of trace heavy metals that are pre-accumulated in iron corrosion scales, since these might pose a health risk if these contaminants are released into drinking water.

Alternative water sources and long distance water transport can help solve water shortage problems. However, source water switches can cause undesirable water quality changes due to the disturbance of corrosion scales by changes in water chemistry. Sulfate was identified as one of the most significant water quality parameters in many water chemical stability models and indices such as the Larson index (Larson and Skold 1958). Under source switch condition, sulfate has been recognized as a causative agent of red water in many cases, and elevated levels of Fe or Mn in bulk water are associated with discolored water (Li *et al.* 2010, Ginige *et al.* 2011). For example, in a red water case caused by source water switch in a northern China city, it was found that the new water source had significantly higher sulfate concentration compared with local water source (200 mg L^{-1} vs 30 mg L^{-1}) (Yang *et al.* 2014), but the effect of sulfate on the deterioration of water quality within DWDS are currently not fully understood.

Moreover, iron release from corrosion scales/deposits in DWDS is usually not considered to be a health concern but rather an aesthetic issue associated with discolored water. Fe and Mn based compounds commonly existing in DWDS corrosion scales are capable of adsorbing and concentrating trace heavy metals. We

wonder if heavy metal release accompanied by iron release could result from switching to alternative source water and long distance transported water. The relationship and the interaction mechanisms between Fe and Mn release and heavy metal release are not well understood. The main factors influencing the release behavior of heavy metals are also not known.

This work sought to identify and evaluate the release of trace heavy metals under switching water quality conditions. Iron pipe sections from actual DWDS with different source water supply histories were collected for pipe loop set-up. The relationships of total iron release, trace heavy metal release and corrosion scale constituents under changing sulfate water conditions were systematically analyzed and discussed.

2. Materials and methods

2.1 Pipe loop set-up and operation

Test cast-iron pipes (approximately 20 years old) were obtained from two locations in a northern city of China, and labelled as Pipe-A and Pipe-B. Historically, Pipe-A was transporting finished surface water (SW1), and Pipe-B was transporting finished groundwater (GW1). Water sources, main finished water quality parameters and treatment processes of the corresponding water treatment plants are summarized in Table S1. Two pipe loop facilities were set up in parallel, and each facility consisted of five DN100 and 1-m-long test pipe sections and three 0.1-m-long coupon pipe sections (Fig. S1). The pipe loops with Pipe-A and Pipe-B were designated as Loop 1

(L1) and Loop 2 (L2), respectively.

A two-phase experiment was conducted for both pipe loops. Phase I: feed water was regular tap water collected from our lab without further disinfection (with low residual chlorine of 0.05-0.07 mg L^{-1}). The sulfate concentration was about 75 mg L^{-1}, and the duration was 50 d (equilibration period for stabilizing the concentration of total iron and turbidity of effluents). Phase II: sulfate concentration of feed water was increased by adding sodium sulfate to the regular tap water. Three sulfate concentrations were applied for each loop: for L1, 200, 250, and 300 mg L^{-1}; for L2, 200, 230, and 250 mg L^{-1}.

Experimental phases, operation conditions, and corresponding water types for each loop are listed in Table 1. We simulated the actual flow mode of water in the distribution system and the domestic use. A complete operation cycle was set at 48 h, and routine operation cycle procedures were as follows: first, a certain amount of test water was prepared in a water tank; then water circulation was started and continued for 36 h, corresponding to 16 h of hydraulic retention time (HRT) in cast-iron pipes; second, circulation was suspended and the water was kept motionless for 8 h, then samples were taken for measurement; at the end, used water was discharged and preparations for a new cycle were started. The 8 h motionless time represented the night status when there was little or no water use. Water was circulated in test pipe loops using a centrifugal pump at a flow rate of 3.2 m^3 h^{-1}, and the flow velocity in test pipe sections was approximately 0.1 m s^{-1}. The water temperature was maintained at 20 ±1°C using a heat-exchanging unit.

155

156 ***2.2 Pipe section reactor set-up and operation***

157 Several small pipe section reactors (Loop 3) were assembled with cast iron pipes,
158 which were harvested from another GW (GW2) service area in a northern city of
159 China (Fig.S2). These pipes (denoted as Pipe-C) were approximately 20 years old,
160 with diameter of DN100. Each test pipe was cut into 0.1-m-long experimental
161 sections, and the cutting faces were coated with epoxy resin to prevent water contact.
162 The HRT in pipe section reactors was 8 h. A stirring device was installed in reactors to
163 simulate water flow conditions in actual DWDS.

164 Raw tap water from the lab was fed into the pipe section reactors until the
165 concentration of total iron and turbidity of effluents stabilized (phase I). Then the
166 sulfate concentration was increased by adding sodium sulfate to the regular tap water
167 at 200, 300, 400, 500, 600 mg L^{-1} (phase II), to evaluate sulfate effects on the release
168 of heavy metals from iron corrosion scales. The test used six concentration gradients
169 (from 75 to 600 mg L^{-1}), and was replicated five times (ran 1~ ran 5).

170

171 ***2.3 Analytical methods***

172 Water quality parameters, such as pH, temperature, dissolved oxygen (DO),
173 conductivity, turbidity, alkalinity, chloride (Cl^-) and SO_4^{2-} were measured for both feed
174 and effluent water. The pH, temperature, DO and conductivity were measured using
175 Portable Multiparameter meter (Sension156 HACH, USA), and the turbidity was
176 measured using a 2100P Turbidimeter (HACH, USA). Free chlorine was measured

using a HACH DR2800 spectrophotometer. SO_4^{2-} and Cl^- were analyzed using the Ion Chromatography System-1000 (Dionex, USA). Fe, Mn, Cu, Zn, Pb, Ni, Cr and As were analyzed by Inductively Coupled Plasma Mass Spectrometer (ICP-MS, Perkin-Elmer Optima 2000, USA). Unless otherwise specified, all chemicals used in this study were Analytical Reagent grade. Ultrapure nitric acid was used to digest samples for metal analysis.

2.4 Characterization of iron corrosion scales

Corrosion scale samples were collected from freshly obtained pipe sections and pipe loops L1 and L2 at the end of phase I and phase II, respectively. Typical corrosion scale samples with different appearances were classified and analyzed separately. Pretreatment procedures were as described previously (Yang *et al.* 2012). X-ray diffraction (XRD, D/max-rA, Rigaku Co., USA) and X-ray Fluorescence (XRF, Advant' XP, Thermo Electron, Switzerland) were performed to characterize the crystalline phase and elemental composition of corrosion scales. The instrumental information for XRD and XRF as well as the quantification method for XRD were the same as described previously (Yang *et al.* 2012).

3. Results and discussion

3.1 Structural and elemental composition of initial corrosion scales

The morphology of corrosion scales on cast iron pipes differed depending on the type of historic source water (Fig. S3), which was described previously (Yang *et al.*

199 2012, Sun *et al.* 2014a). According to Yang *et al.* (2014), corrosion scales on pipes
200 historically transporting treated SW (Pipe-A) with an appearance of a continuous
201 thick layer (10-20 mm) could be divided into top surface and hard shell (THS), porous
202 core layers (PCL), and entire tubercle (ET). THS and ET scales are at the interface
203 between bulk water and the pipe wall, and were barriers that protected the pipe from
204 further corrosion. Their stability changes have great impact on iron corrosion and
205 metal release. Scales on pipes transporting GW (Pipe-B and Pipe-C) are relatively
206 thin (only few millimeters or less than a millimeter) with non-tubercle-formed
207 corrosion scale (TNCS). The hollow tubercle (HT), scale type which formed in the
208 pipes transporting GW, was not detected in the present study.

209 A total of 22 inorganic elements (including Fe, Si, Ca, Al, Na, Mg, S, K, Mn, P, Ti,
210 Zn, Cl, Mo, Ni, Cr, V, Sr, Cu, Pt, Pb and As) in DWDS corrosion scales were detected
211 in the corrosion scale samples. Table 2 summarizes the contents ($\mu g\ g^{-1}$) of some main
212 elements in the initial corrosion scales. Fe was the largest component in all of the
213 scales analyzed, with mean content of 519640 $\mu g\ g^{-1}$. The second most abundant
214 element for the two scales of TNCS was Ca (mean = 22100 $\mu g\ g^{-1}$), and nearly 6.5
215 times of the Ca content in THS, PCL and ET (mean = 3424 $\mu g\ g^{-1}$). As, Cr, Cu, Mg,
216 Mn, Pb and Zn also had higher levels in TNCS, compared with other scale samples.
217 The contents of S in the THS, PCL and ET scales were greater than those in the two
218 scales of TNCS, and the highest content was present in the PCL scale. S occurrence in
219 scales is likely to be in the form of troilite, a common under-layer component of iron
220 corrosion scales (Benjamin *et al.*, 1996). We did not detect crystalline Fe_xS_y minerals

221 by XRD, but the XRF results demonstrated that S was common.

222

223 ***3.2 Heavy metal release***

224 Inorganic contaminants in DWDS solids came from several sources, but mainly
225 from source water and pipe materials. According to Peng *et al.* (2012), As, V and U
226 released from mineral deposits dissolution were more prevalent in GW supplies, since
227 they could not be efficiently removed by traditional water treatment plants. Some
228 other metal ions such as Pb, Cu, Cd, Cr and other impurities might originate from pipe
229 materials and pipe joints in DWDS (Masters *et al.* 2016). We studied the effects of
230 sulfate on seven heavy metals (including As, Cr, Cu, Mn, Ni, Pb and Zn) release using
231 cast iron pipe-loops with different corrosion scales. The changes of heavy metal
232 release under different sulfate concentrations are presented in Fig. 1. Releases of As,
233 Cr, Cu, Mn, Ni and Pb increased immediately at higher sulfate concentration but the
234 releases gradually decreased over time. Compared with L1, the releases of As, Cu, Mn,
235 Ni and Pb in L2 were greater. In pipe section reactors (L3), heavy metal release
236 exhibited similarity to L1 and L2. The mean concentrations of these heavy metals
237 under different sulfate concentrations are show in Table 3. There was no correlation
238 between Zn release and sulfate concentration in all pipe loops (reactor).

239 ***Mn.*** Mn occurrence in corrosion scales was mainly due to the formation and
240 deposition of Mn oxyhydroxide that originated from the source water (Peng *et al.*
241 2010, Swietlik *et al.* 2011). Under anoxic environments, Mn
242 oxides/oxyhydroxides were prone to reduction and re-solubilization, with associated

243 release of adsorbed substance (e.g. As, Pb, Ni, Cd, Cu, V) (Hill *et al.* 2010). As shown
244 in Fig. 1, higher sulfate levels can cause higher release of Mn. Further correlation
245 analyses (Fig. S4) indicated that Mn release was positively related to sulfate
246 concentration in all pipe loops (R^2: L1 = 0.72; L2 = 0.59). The mean effluent
247 concentrations of Mn in L1 (154 μg L^{-1}), L2 (115 μg L^{-1}) and L3 (117 μg L^{-1}) all
248 exceeded the drinking water standards of China (100 μg L^{-1}, GB 5749-2006), when
249 the sulfate concentration increased to 300 mg L^{-1}, 230 mg L^{-1} and 300 mg L^{-1},
250 respectively (Fig. 1, Table 3). XRF results demonstrated that the contents of Mn in
251 THS, PCL, ET and TNCS (L2) decreased at higher sulfate water levels, and the
252 decrements were 194, 233, 258 and 443 μg L^{-1}, respectively (Table 2). The oxygen
253 consumption for L1 and L2 also increased with sulfate, especially for L2 (Fig. S5).
254 For example, the residual DO concentration decreased rapidly from 6.67 to 0.98 mg
255 L^{-1} in L2, when the pipe loop operated for 8 h (an entire operation cycle was 48 h),
256 which was much lower than that of L1 (3.65 mg L^{-1} after 26 h operation). Therefore,
257 when switching to higher sulfate water, the anaerobic condition might contribute to
258 the release of Mn in reduced and more soluble form, which needs to be confirmed.

259 ***Ni***, ***Cu***. Similar to Mn release, elevated levels of Ni and Cu were found in all pipe
260 loops when initially increasing sulfate concentration (Fig.1, Table 3). The
261 concentrations of Ni in L2 (22 μg L^{-1}) and L3 (23 μg L^{-1}) also exceeded the drinking
262 water standards (20 μg L^{-1}), when the sulfate concentrations increased to 250 mg L^{-1}
263 (L2) and 400 mg L^{-1} (L3), respectively. XRF results showed that the contents of Ni
264 and Cu both decreased, sometimes to undetectable levels, in most of the scales at

265 phase II (Table 2). A strong positive relationship existed between the release of Ni and
266 Mn (R^2: L1 = 0.95, L2 = 0.90), while relatively weak correlation existed between the
267 release of Ni and sulfate (R^2: L1 = 0.73, L2 = 0.65) (Fig. S4). Shi *et al.* (2007) found
268 that Cu release was controlled by the dissolution of the corrosion scales, not by the
269 corrosion rate of the metal. Mn-containing deposits could absorb Cu in DWDS, and
270 the destabilization/re-solubilization of Mn deposits might increase the Cu ions in
271 consumer taps (Gerke *et al.* 2016). Cu release was strongly correlated with Mn release
272 (R^2: L1 = 0.82, L2 = 0.97), but weakly correlated with sulfate (R^2: L1 = 0.53, L2 =
273 0.50) (Fig. S4). Mn compounds can also absorb Ni effectively (Trivedi *et al.* 2001).
274 Hence, it might indicate that the release of Cu and Ni were mainly accompanied by
275 the release of Mn under higher sulfate condition.

276 ***As***, ***Cr***, ***Pb***. Under raw tap water condition, the effluent concentrations of As and Cr
277 were very low, and often undetectable. At higher sulfate water levels, the release of As
278 and Cr increased but remained lower than their influent concentrations (Fig. 1, Table
279 3). As release was positively correlated with Mn release (R^2: L1 = 0.78, L2 = 0.75),
280 while Cr release was more associated with sulfate levels (R^2: L1 = 0.86, L2 = 0.84)
281 (Fig. S4). Pb release clearly increased with sulfate level. But under raw tap water
282 condition, Pb release was also lower than its influent concentration. A strong positive
283 correlation existed between the release of Pb and Mn (R^2: L1 = 0.94, L2 = 0.91), and
284 relative weak relationship existed between Pb release and sulfate level (Fig. S4). In
285 the presence of high concentrations of sulfate water, the contents of As, Cr, and Pb in
286 all analyzed scales decreased (Table 2). The ability for iron oxides to adsorb As is

287 well-known, and compounds commonly found in iron corrosion scales (such as
288 α-FeOOH, γ-FeOOH, Fe_3O_4 *et al.*) have similar adsorptive properties, which could
289 therefore concentrate As and potentially release it into the DWDS (Lytle *et al.* 2004).
290 Mn oxides/oxhydroxides on pipe internal surfaces or iron corrosion scales also can
291 effectively adsorb Cr, Cu, Pb *et al.* (Lytle *et al.* 2004, Gerke *et al.* 2016, Manceau *et*
292 *al.* 1992). Therefore, we suspect that the adsorption of As, Cr and Pb by Fe/Mn based
293 solids within corrosion scales accounts for their relatively lower effluent
294 concentrations. Moreover, Mn oxides could oxidize some adsorbed metal ions, e.g.,
295 Cr (III) to Cr (VI), changing the toxicity of the heavy metals (Gerke *et al.* 2016). Cr
296 (IV) bound to Mn oxides/oxhydroxides and ingested is a potential human health risk.
297

298 ***3.3 Iron release and relationships between iron and heavy metal release***

299 Curves of total iron release for L1 and L2 exhibited similar variation during the
300 entire experimental period (Fig. 2). The total iron concentrations increased at the
301 initial stage with increasing sulfate concentration, and then decreased with time (in
302 accord with the results observed in L3, see below). Compared to L1, total iron release
303 in L2 was greatly affected by sulfate concentration. The concentrations of total iron in
304 L2 nearly all exceeded 0.3 mg L^{-1} (upper limit of the drinking water standard for iron
305 in China) when switching to higher sulfate water, and the effluents always exhibited a
306 yellowish color. The total iron release fluctuation scenarios ("Δ total iron release" =
307 "total iron release sample measurement" minus "average total iron release in
308 corresponding experimental phase") under different sulfate concentrations for L1 and

L2 are illustrated in Fig. S6. The "Δ total iron release" for L2 changed over a wider range from -0.057 ~ 0.076 mg L^{-1} (phase I) to -0.078 ~ 0.069 mg L^{-1}, -0.120 ~ 0.182 mg L^{-1} and -0.170 ~ 0.290 mg L^{-1}, when the sulfate concentration increased to 200, 230 and 250 mg L^{-1}, respectively. However, the "Δ total iron release" for L1 had a narrower range of between -0.053 ~ 0.090 mg L^{-1} during the entire experimental phases. The total iron release fluctuation scenarios under various operation conditions can reflect pipe scale stability (Yang *et al.* 2014). These results demonstrated that the corrosion scales of GW pipes were more affected by sulfate and the corrosion scale stability of SW pipes was higher than that of GW pipes, since the same water matrix (lab tap water) was used in this study and the change in water quality was only the level of sulfate.

Sulfate is often the causative agent of red water, and this is reflected in indices such as the Larson index (Li *et al.* 2010). Sulfate can increase ferrous iron diffusion from pipe surfaces into bulk water, resulting in increased iron concentrations, but the pathways involved are not well understood. In the present study, we found that increasing sulfate concentration leads to a relatively anaerobic environment in distribution systems (especially for GW pipes). For L2, the DO concentration decreased rapidly from 6.67 to 0.98 mg L^{-1} when the sulfate concentration increased to 250 mg L^{-1}. However, the concentration of DO in L1 decreased slowly from 6.67 to 3.65 mg L^{-1}, even when the sulfate concentration increased to 300 mg L^{-1}. According to the Kuch mechanism, it is possible for previously deposited ferric scales to act as an electron acceptor and produce ferrous iron to diffuse into water in the absence of

oxygen (Eqn.1) (Kuch *et al.* 1998). Sarin *et al.* also reported that decreasing the oxidant concentrations, such as DO, in water can increase the amount of iron release from corroded iron pipes (Sarin *et al.* 2004). Therefore, the anaerobic condition caused by increased sulfate concentrations could be an important factor increasing total iron release.

$$Fe_{(metal)} + 2FeOOH_{(scale)} + 2H^{+} \rightarrow 3Fe^{2+} + 4OH^{-} \quad (1)$$

Total iron release for L3 was similar to L1 and L2 when sulfate concentration increased (Fig. 3). Under a fixed sulfate concentration, total iron release in ran 1 was greater than that in ran 2, and ran 2 was greater than ran 3. The total iron concentrations in ran 3, ran 4, and ran 5 were closer. The reason for this might be the contents of iron oxides, which can be easily released into the water, decreased over time. Sulfate could cause a more protective scale on the pipe surface, or change the corrosion scales from less stable to more stable constituents (Yang *et al.* 2014, Imran *et al.* 2006, McNeill and Edwards 2001). In the present study, the contents of stable iron components, such as α-FeOOH and Fe_3O_4 all increased over time in the presence of higher sulfate water concentration, and this also could account for the gradual lowering of iron release. The following section provides corrosion scale comparison and discussion.

The total iron release was positively correlated with sulfate both in L1 (R^2 = 0.70) and L2 (R^2 = 0.58) (Fig. 4). Strong positive correlations also existed between the release of Fe & Mn, Fe & Ni, Fe & Cu, and Fe & Pb, with R^2 all being greater than 0.8. Compared to other heavy metals, Cr release was more closely related to sulfate

353 level (R^2: L1 = 0.86, L2 = 0.84) and As release was correlated to Mn release (R^2: L1 =
354 0.78, L2 = 0.75). This suggests that total iron release triggered by sulfate could result
355 in pre-accumulated/adsorbed heavy metal release back into the drinking water.
356 Therefore, the total iron release not only contributed to discolored water, but was also
357 a health concern with concomitant heavy metal release into DWDS.
358
359 ***3.4 Effect of corrosion scale composition transformation on heavy metal release***
360 Corrosion scales with different morphologies were collected from newly obtained
361 pipe sections in L1 - L3 under different experimental phases, and the crystalline
362 phases were characterized by XRD (Fig. 5). For the initial corrosion scale samples
363 (from pipe sections in phase I), α-FeOOH and Fe_3O_4 were the main constituents of
364 THS and ET. Relatively higher content of unstable iron components, such as
365 γ-FeOOH, siderite ($FeCO_3$), green rust ($Fe_6(OH)_{12}CO_3$, GR) and amorphous iron
366 oxides existed in PCL. For the two scales of TNCS, amorphous iron oxides were in
367 greatest abundance, but the contents of α-FeOOH were relatively lower compared
368 with THS and ET.
369 After moving to a higher sulfate water concentration, some notable characteristics
370 of the transformation of scale crystalline composition were observed. First, the
371 relatively abundance of Fe_3O_4 in all kinds of corrosion scales increased when at
372 higher sulfate levels and the increased percentages were all > 10% except PCL (6%).
373 The relative contents of α-FeOOH increased in all samples by 2% - 4%. Sulfate was
374 deemed to increase iron corrosion, and accelerate the formation of ferrous iron from

375 elemental iron (Eqn. 2). Ferrous iron can be oxidized by DO to form α-FeOOH and
376 Fe_3O_4 under low oxidation rates (Eqn. 3-5), according to the Siderite model proposed
377 by Sontheimer *et al.* (1981).

378 $$Fe\ (s) \rightarrow Fe^{2+} + 2e^- \quad (2)$$

379 $$2Fe^{2+} + 1/2\ O_2 + 4OH^- \rightarrow 2\alpha\text{-}FeOOH + H_2O \quad (3)$$

380 $$2FeCO_3 + 1/2\ O_2 + 4OH^- \rightarrow 2\alpha\text{-}FeOOH + CO_2 \quad (4)$$

381 $$2FeCO_3 + 1/2\ O_2 \rightarrow Fe_3O_4 + CO_2 \quad (5)$$

382 Equations 3 to 5 are oxidation reactions, which could promote the formation of
383 α-FeOOH and Fe_3O_4 by consuming DO, and lead to an anaerobic environment in
384 DWDS. Several studies have reported that ferric hydroxides (e.g., α-FeOOH,
385 β-FeOOH, γ-FeOOH and amorphous ferric oxyhydroxides) can be converted to Fe_3O_4
386 by iron reducing bacterial (IRB) under anaerobic condition (Lovley 1998, Roh *et al.*
387 2003, Sun *et al.* 2014b). In the present study, the bacterial communities in scale
388 samples were analyzed by 16S rRNA pryosequencing (Supplementary materials A).
389 Results showed that the relative abundances of IRB in all corrosion scales also
390 increased when switching to higher sulfate water (Fig.S7, Table S3). The high
391 abundance of IRB in scales could favor the formation and preservation of Fe_3O_4.
392 Fe_3O_4 is thermodynamically stable, which could produce a dense and compact
393 corrosion scale. Corrosion scales with high Fe_3O_4 content usually possesses protective
394 and anti-corrosive properties, which serve as barriers hindering the diffusion of
395 corrosive ions into corrosion scales (Sarin *et al.* 2001, Sarin *et al.* 2004, Lytle *et al.*
396 2005). Fe_3O_4 is also an effective sorbent for some heavy metals such as Cu, Pb, Cr, As

(Rajput *et al.* 2016, Yantasee *et al.* 2007, Hu *et al.* 2004). Therefore, Fe_3O_4 could act as a barrier to hinder the release of heavy metals on the one hand, and also to act as a sink to adsorb released heavy metals. The formation of Fe_3O_4 might be one of the most important factors for inhibiting the release of total iron and heavy metals.

Second, the percentages of some unstable ferric or ferrous iron oxides (including β-FeOOH, γ-FeOOH and $FeCO_3$ and amorphous iron oxides) in THS, ET, and two samples of TNCS all decreased when switching to higher sulfate water. The decreased percentages were all > 10%. β-FeOOH, γ-FeOOH, $FeCO_3$ and amorphous iron oxides were chemically unstable, and the relatively higher percentage of these in corrosion scales indicated the weak tolerance of distribution pipes to feed water chemistry changes (Yang *et al.* 2014). Therefore, the decrease of these unstable ferric or ferrous iron oxides means that the iron corrosion scales in pipe loops tend to be more stable, which could also account for the decreased release of heavy metals over time.

Third, we found that when switching to higher sulfate water, the relative abundance of GR in THS decreased from 15% to 8%, while the contents of GR in the two samples of TNCS both increased (L2: from 16% to 26%, L3: from 16% to 28%). GR was chemically unstable, and could be oxidized by dissolved oxygen into Fe_3O_4, α-FeOOH, γ-FeOOH and γ-Fe_2O_3, depending on pH and oxidation rate (Pineau *et al.* 2008). Under anaerobic condition (as in L2 at phase II), GR can remain for a long time (Refait *et al.* 3003). The higher abundance of these unstable ferrous oxides could lead to more serious heavy metal release in DWDS. This might explain why the release of total iron and some heavy metals were more serious in L2 than those in L1.

GR and sulfate reducing bacterial (SRB) always coexisted, due to the presence of GR, and this could favor the colonization of SRB (Refait *et al.* 2003). Bacterial community analyses showed that the relatively abundance of SRB in all corrosion scales increased under higher sulfate concentration, especially in the two samples of TNCS (Fig.S7, Table S3). SRB were usually associated with anaerobic iron corrosion, which could favor sulfide production and thus promote iron corrosion and ferrous iron formation (Lytle *et al.* 2005, Pineau *et al.* 2008). However, SRB could use sulfate as an electron acceptor and generate sulfide (S^{2-}) in an anaerobic environment, the biogenically produced S^{2-} could react with dissolved metals to form metal sulfide precipitates, such as Cu, Zn, Ni, Fe, Al, As and Mn (Jong *et al.* 2003). Therefore, the growth of SRB could also decrease heavy metal release.

4. Conclusions

Changes in water chemistry can result in accumulated/adsorbed trace heavy metals in iron corrosion scales being released back into domestic water supplies thus leading to reduced water quality. The present work systematically investigated the effect of sulfate on the release of trace heavy metals from iron corrosion scales to bulk water.

The release of Mn, Ni, Cu, Pb, Cr and As from iron corrosion scales increased immediately after sulfate concentration increased and then gradually decreased over time. Pipes historically transporting GW had greater heavy metal release, compared with pipes historically transporting SW. Significant correlations ($R^2 > 0.8$) existed between the release of Fe & Mn, Fe & Ni, Fe & Cu, and Fe & Pb in all pipe loops.

441 Mn release was also associated with other metals, and positive correlations existed
442 between Mn & Ni (R^2: L1 = 0.95, L2 = 0.90), Mn & Pb (R^2: L1 = 0.94, L2 = 0.91),
443 Mn & Cu (R^2: L1 = 0.82, L2 = 0.97) and Mn & As (R^2: L1 = 0.79, L2 = 0.75).
444 For the pipes historically transporting SW, corrosion scales tended to be more stable
445 in the presence of higher sulfate levels, with a larger proportion of stable constituents
446 (mainly Fe_3O_4) and fewer unstable compounds (β-FeOOH, γ-FeOOH, $FeCO_3$ and
447 amorphous iron oxides). The main functional bacterial communities IRB were
448 favorable for the formation of Fe_3O_4. For pipes historically transporting GW,
449 constituents of corrosion scales also achieved more stability, while the anaerobic
450 condition promoted the formation of GR, a main precursor of stable iron constituents.
451 The higher metal release in pipes transporting GW can be partially attributed to the
452 higher GR content. The relative abundance of SRB increased with sulfate
453 concentration in all kinds of scales. The transformation of corrosion scales to a more
454 stable state and the growth of SRB may explain the gradual decrease of heavy metal
455 release over time.
456

457 ## Acknowledgments

458 This work was supported by the National Natural Science Foundation of China
459 (51378493) and the National Water Pollution Control and Treatment Special Key
460 Project of China (2012ZX07404-002).

461 ## **Appendix A.** Supplementary data

462 Supplementary data related to this study is provided in Supplementary Materials

A.

References

Benjamin, M.M, Sontheimer, H., Leroy P., 1996. Corrosion of Iron and Steel. In Internal Corrosion of Water Distribution Systems. Cooperative Research Report. AWWA Research Foundation, Denver, CO, pp. 29-70.

Fisher, E.L., Fuortes, L.J., Valentine, R.L., Mehrhoff, M. and Field, R.W., 2000. Dissolution of 226 Radium from pipe-scale deposits in a public water supply. Environment International 26 (1-2), 69-73.

Gerke, T.L., Little, B.J. and Maynard, J.B., 2016. Manganese deposition in drinking water distribution systems. Science of the Total Environment 541 (110), 184-193.

Ginige, M.P., Wylie, J. and Plumb, J., 2011. Influence of biofilms on iron and manganese deposition in drinking water distribution systems. Biofouling 27 (2), 151-163.

Hill, A.S., Friedman, M.J., Reiber, S.H., Korshin, G.V. and Valentine, R.L., 2010. Behavior of trace inorganic contaminants in drinking water distribution systems. Journal American Water Works Association 102 (7), 107-118.

Hu, J., Lo, I.M.C. and Chen, G., 2004. Removal of Cr(VI) by magnetite. Water Science & Technology 50 (12), 129-146.

Imran, S.A., Dietz, J.D., Mutoti, G., Xiao, W.Z., Taylor, J.S. and Desai, V., 2006. Optimizing source water blends for corrosion and residual control in distribution systems. Journal American Water Works Association 98 (5), 107-115.

Jong, T. and Parry, D.L., 2003. Removal of sulfate and heavy metals by sulfate reducing bacteria in short-term bench scale upflow anaerobic packed bed reactor runs. Water Research 37 (14), 3379-3389.

Kuch, A., 1988. Investigations of the reduction and reoxidation kinetics of iron (III) oxide scales formed in waters. Corrosion Science 28 (3), 221-231.

Larson, T.E. and Skold, R.V., 1985. Laboratory studies relating mineral quality of water to corrosion of steel and cast iron. Journal of American Water Works Association 14 (6), 285-288.

Li, D., Li, Z., Yu, J., Cao, N., Liu, R. and Yang, M., 2010. Characterization of Bacterial Community Structure in a Drinking Water Distribution System during an Occurrence of Red Water. Applied and Environmental Microbiology 76 (21), 7171-7180.

Lovley, D.R., 1998. Geomicrobiology: Interactions between microbes and minerals. Science 280 (5360), 54-55.

Lytle, D.A., Gerke, T.L. and Maynard, J.B., 2005. Effect of bacterial sulfate reduction on iron-corrosion scales. Journal American Water Works Association 97 (10), 109-120.

Lytle, D.A., Sorg, T.J. and Frietch, C., 2004. Accumulation of arsenic in drinking water distribution systems. Environmental Science & Technology 38 (20), 5365-5372.

Lytle, D.A., Sorg, T.J., Muhlen, C. and Wang, L.L., 2010. Particulate arsenic release in a drinking water distribution system. Journal American Water Works Association 102 (3), 87-98.

Manceau, A., Charlet, L., Boisset, M.C., Didier, B. and Spadini, L., 1992. Clays and Hydrosilicate Gels in Nuclear Fields Sorption and speciation of heavy metals on hydrous Fe and Mn oxides. From microscopic to macroscopic. Applied Clay Science 7 (1), 201-223.

Masters, S., Welter, G.J. and Edwards, M., 2016. Seasonal Variations in Lead Release to Potable Water.

Environmental Science & Technology 50 (10), 5269-5277.

McNeill, L.S. and Edwards, M., 2001. Iron pipe corrosion in distribution systems. Journal American Water Works Association 93 (7), 88-100.

Peng, C.Y., Hill, A.S., Friedman, M.J., Valentine, R.L., Larson, G.S., Romero, A.M.Y., Reiber, S.H. and Korshin, G.V., 2012. Occurrence of trace inorganic contaminants in drinking water distribution systems. Journal American Water Works Association 104 (3), 53-54.

Peng, C.-Y., Korshin, G.V., Valentine, R.L., Hill, A.S., Friedman, M.J. and Reiber, S.H., 2010. Characterization of elemental and structural composition of corrosion scales and deposits formed in drinking water distribution systems. Water Research 44 (15), 4570-4580.

Pineau, S., Sabot, R., Quillet, L., Jeannin, M., Caplat, C., Dupont-Morral, I. and Refait, P., 2008. Formation of the Fe(II-III) hydroxysulphate green rust during marine corrosion of steel associated to molecular detection of dissimilatory sulphite-reductase. Corrosion Science 50 (4), 1099-1111.

Rajput, S., Pittman, C.U. and Mohan, D., 2016. Magnetic magnetite (Fe_3O_4) nanoparticle synthesis and applications for lead (Pb^{2+}) and chromium (Cr^{6+}) removal from water. Journal of Colloid and Interface Science 468, 334-346.

Refait, P., Memet, J.B., Bon, C., Sabot, R. and Génin, J.M.R., 2003. Formation of Fe (II) - Fe (III) hydroxysulphate green rust during marine corrosion of steel. Corrosion Science 45 (4), 833-845.

Reiber, S. and Dostal, G., 2000. Well Water Disinfection Sparks Surprises . Opflow. 26 (3), 1, 4-6, 14.

Roh, Y., Zhang, C.L., Vali, H., Lauf, R.J., Zhou, J. and Phelps, T.J., 2003. Biogeochemical and environmental factors in Fe biomineralization: Magnetite and siderite formation. Clays and Clay Minerals 51 (1), 83-95.

Schock, M.R., Hyland, R.N. and Welch, M.M., 2008. Occurrence of contaminant accumulation in lead pipe scales from domestic drinking-water distribution systems. Environmental Science & Technology 42 (12), 4285-4291.

Sarin, P., Snoeyink, V.L., Bebee, J., Jim, K.K., Beckett, M.A., Kriven, W.M. and Clement, J.A., 2004. Iron release from corroded iron pipes in drinking water distribution systems: effect of dissolved oxygen. Water Research 38 (5), 1259-1269.

Sarin, P., Snoeyink, V.L., Bebee, J., Kriven, W.M. and Clement, J.A., 2001. Physico-chemical characteristics of corrosion scales in old iron pipes. Water Research 35 (12), 2961-2969.

Shi, B.Y. and Taylor, J.S., 2007. Iron and copper release in drinking-water distribution systems. Journal of Environmental Health 70 (2), 29-36.

Sontheimer, H., Kolle, W. and Snoeyink, V.L., 1981. The siderite model of the formation of corrosion-resistant scales. Journal American Water Works Association 73 (11), 572-579.

Sun, H., Shi, B., Bai, Y. and Wang, D., 2014a. Bacterial community of biofilms developed under different water supply conditions in a distribution system. Science of the Total Environment 472 (1), 99-107.

Sun, H., Shi, B., Lytle, D.A., Bai, Y. and Wang, D., 2014b. Formation and release behavior of iron corrosion products under the influence of bacterial communities in a simulated water distribution system. Environmental science. Processes & impacts 16 (3), 576-585.

Swietlik, J., Raczyk-Stanislawiak, U., Laskowski, T. and Nawrocki, J., 2011. Model Investigations into the Migration of Some Elements from Cast Iron and Steel into Water Due to Pipe Corrosion. Ochrona Środowiska 33 (3), 71-76.

Trivedi, P., Axe, L. and Tyson, T.A., 2001. XAS studies of Ni and Zn sorbed to hydrous manganese oxide. Environmental Science & Technology 35 (22), 4515-4521.

549 Yang, F., Shi, B., Bai, Y., Sun, H., Lytle, D.A. and Wang, D., 2014. Effect of sulfate on the
550 transformation of corrosion scale composition and bacterial community in cast iron water
551 distribution pipes. Water Research 59 (4), 46-57.
552 Yang, F., Shi, B., Gu, J., Wang, D. and Yang, M., 2012. Morphological and physicochemical
553 characteristics of iron corrosion scales formed under different water source histories in a drinking
554 water distribution system. Water Research 46 (16), 5423-5433.
555 Yantasee, W., Warner, C.L., Sangvanich, T., Addleman, R.S., Carter, T.G., Wiacek.,R.J., Fryxell, G.F.,
556 Timchalk, C. and Warner, M.G., 2007. Removal of Heavy Metals from Aqueous Systems with Thiol
557 Functionalized Superparamagnetic Nanoparticles. Environmental Science & Technology 42 (14),
558 5114-5119.

Tables

Table 1. Pipe ID, water sources in each pipe loop, experimental conditions and feed water type

Pipe loop	Test pipe	Historic source water	Phases	Duration	Water type	Sulfate (mg L^{-1})
Loop 1	Pipe-A	SW1	I	1-50 d	Tap water	75
			II	52-86 d 88-122 d 124-174 d	Simulated water	200 250 300
Loop 2	Pipe-B	GW1	I	1-50 d	Tap water	75
			II	52-86 d 88-122 d 124-174 d	Simulated water	200 230 250
Loop 3	Pipe-C	GW2	I	7 d	Tap water	75
			II	25 d	Simulated water	200 300 400 500 600

Table 2. Elemental composition of corrosion scales under different experimental conditions (μg/g)

Scale sample ID	Experimental phase	Al	As	Ca	Cu	Cr	Fe	Mg	Mn	Ni	Pb	S	Si	Zn
L1 tap water-THS[a]	Phase I	2350	11	1870	22	26	535500	1470	912	114	20	5910	6680	207
L1 tap water-PCL[b]	Phase I	1870	NA[e]	473	48	40	562600	1140	406	65	31	15300	13700	68
L1 tap water-ET[c]	Phase I	2410	NA	7930	50	35	522100	973	881	39	NA	7540	12900	193
L2 tap water-TNCS[d]	Phase I	1950	47	22800	79	67	514000	3080	1220	82	69	1780	15900	533
L3 tap water-TNCS	Phase I	10400	NA	21400	68	59	464000	3420	1200	85	58	2030	10300	362
L1 simulated water-THS	Phase II	2610	NA	3910	NA	NA	531200	686	718	NA	NA	6530	9380	111
L1 simulated water-PCL	Phase II	2380	NA	195	NA	18	570500	659	173	NA	NA	18100	11100	36
L1 simulated water-ET	Phase II	2350	NA	8390	26	31	529000	604	623	27	NA	7640	11400	132
L2 simulated water-TNCS	Phase II	4100	NA	20800	39	NA	526100	1420	777	NA	29	3970	19500	239
L3 simulated water-TNCS	Phase II	9700	NA	22320	NA	NA	497000	1657	446	NA	16	4330	17300	97

[a] THS: top surface and hard shell; [b] PCL: porous core layer; [c] ET: entire tubercle without layered structure; [d] TNCS: thin corrosion scales; [e] NA: no analyzed

Table 3. Mean values of heavy metal concentrations of influents and effluents in pipe section reactors (L3) under different sulfate concentrations

Pipe loop	Water type	SO_4^{2-} (mg L^{-1})	Metal concentration (μg L^{-1})						
			Mn	Cu	Zn	Pb	Ni	Cr	As
	Influents	75	34	20	50	3.4	5.3	3.4	2.0
L3	Effluents	75	68	25	48	3.1	5.2	2.7	1.3
		200	75	26	49	3.6	10.3	2.8	1.5
		300	117	31	53	3.9	16.4	2.8	1.5
		400	137	44	51	5.0	22.8	2.9	1.6
		500	168	55	49	5.7	28.3	3.0	1.8
		600	180	60	56	7.0	34.3	3.7	2.0

Figure captions

Fig. 1 Changes of heavy metal release in L1 and L2 with time under different sulfate concentrations (a) Mn, (b) Cu, (c) Ni, (d) Pb, (e) Cr, (f) As, (g) Zn

Raw tap water: 2 ~ 50 d, SO_4^{2-} 75 mg L^{-1};

Higher sulfate water: (1) 52 ~ 86 d, SO_4^{2-}: 200 mg L^{-1}; (2) 88 ~ 122 d, SO_4^{2-}: 250 mg L^{-1} (L1), 230 mg L^{-1} (L2); (3) 124 ~ 174 d, SO_4^{2-}: 300 mg L^{-1} (L1), 250 mg L^{-1} (L2)

Fig. 2 Total iron release of L1 and L2 under different sulfate concentrations

Fig. 3 Total iron release of L3 under different sulfate concentrations

Fig. 4 Relationships between the concentrations of total iron & sulfate/Mn (a: L1, b: L2) and total iron & heavy metals (c: L1, d: L2)

The small plots (c1, d1) in (c) and (d) are the enlarged views of the relationships between the concentrations of Fe & As, Fe & Cr and Fe & Pb.

Fig. 5 Crystalline composition variation of THS, PCL, ET and TNCS combined samples for pipe loops L1-L3 under different experimental conditions

(a) Fe_3O_4, (b) α-FeOOH, (c) β-FeOOH / γ-FeOOH / $FeCO_3$, (d) Amorphous iron oxide, (e) $Fe_6(OH)_{12}CO_3$

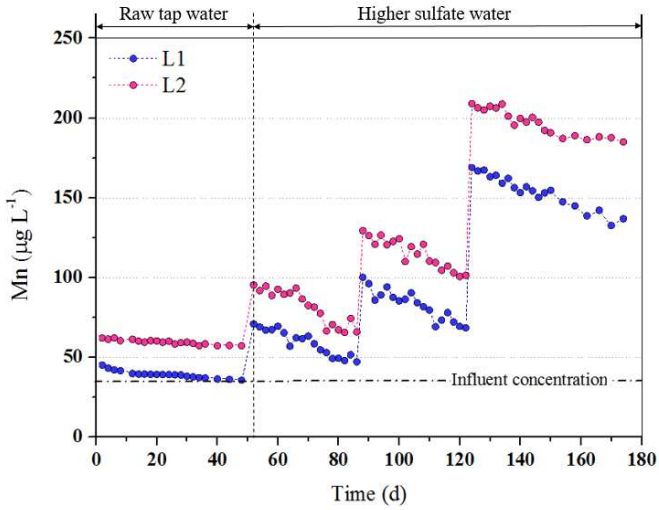
Raw tap water
Higher sulfate water
L1
L2
Influent concentration
Mn (μg L-1)
Time (d)

(a)

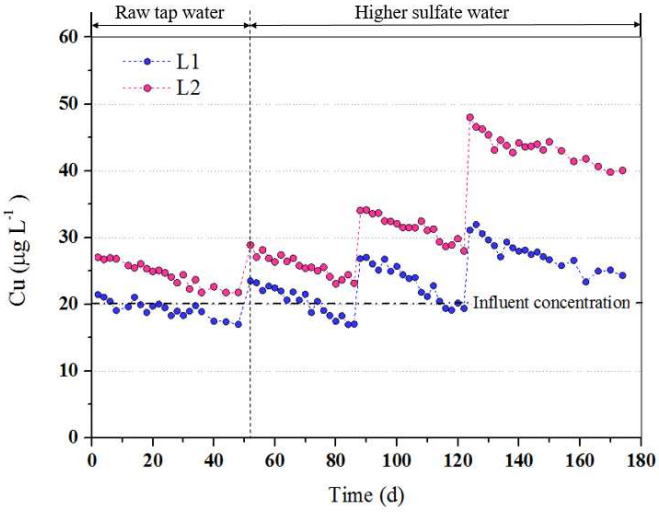
Raw tap water
Higher sulfate water
L1
L2
Influent concentration
Cu (μg L-1)
Time (d)

(b)

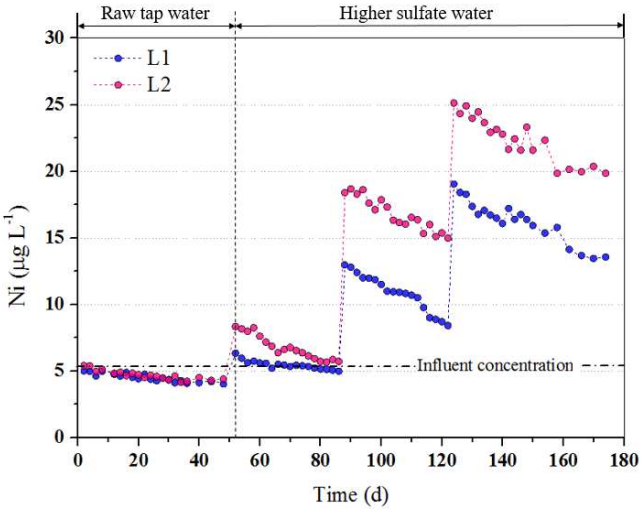
Raw tap water
Higher sulfate water
L1
L2
Influent concentration
Ni (μg L-1)
Time (d)

(c)

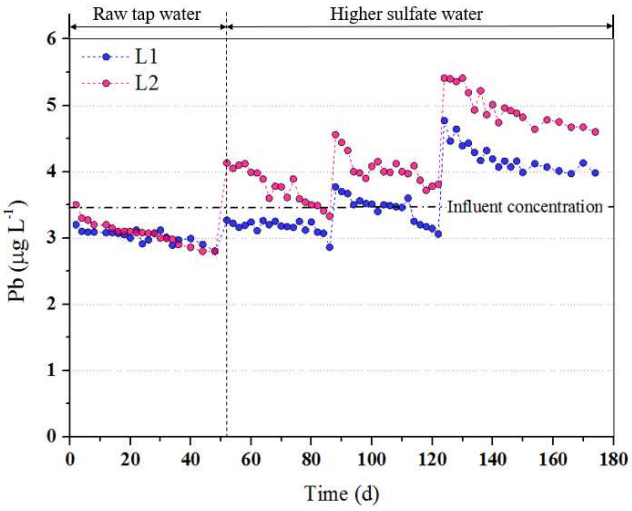
Raw tap water
Higher sulfate water
L1
L2
Influent concentration
Pb (μg L-1)
Time (d)

(d)

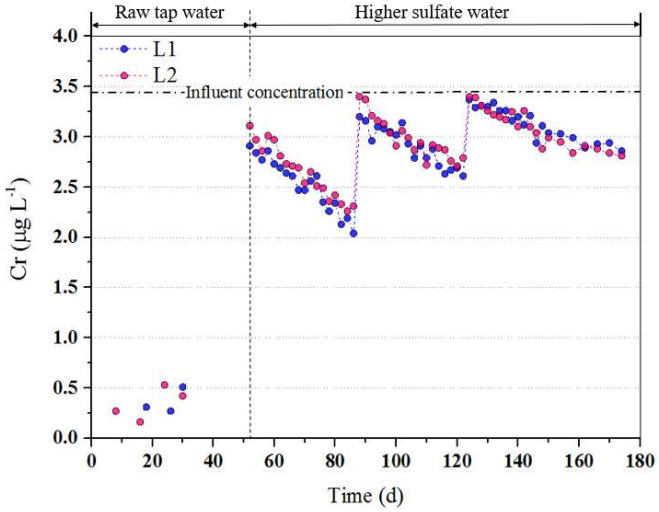
Raw tap water
Higher sulfate water
L1
L2
Influent concentration
Cr (μg L-1)
Time (d)

(e)

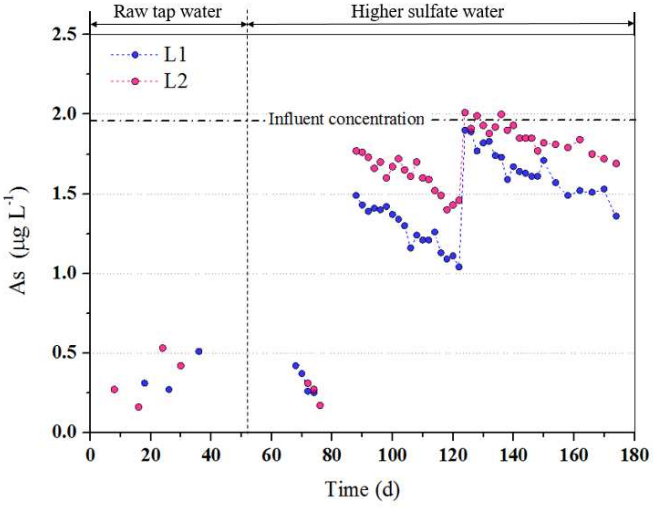
Raw tap water
Higher sulfate water
L1
L2
Influent concentration
As (μg L-1)
Time (d)

(f)

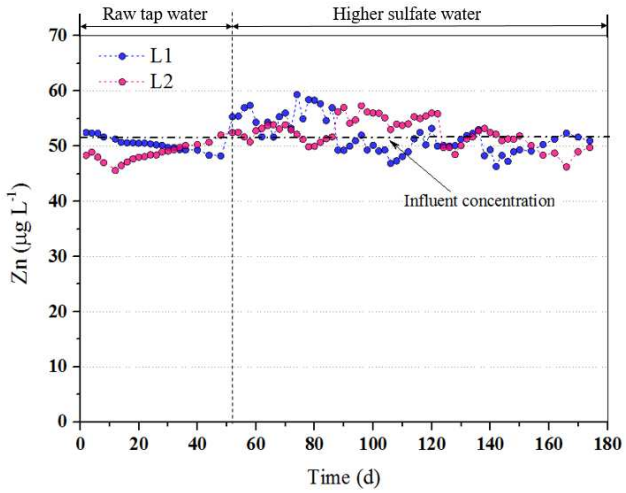

(g)

Fig. 1 Changes of heavy metal release of effluents in L1 and L2 under different sulfate concentrations (a) Mn, (b) Cu, (c) Ni, (d) Pb, (e) Cr, (f) As, (g) Zn

Raw tap water: 2 ~ 50 d, SO_4^{2-}: 75 mg L^{-1};

Higher sulfate water: (1) 52 ~ 86 d, SO_4^{2-}: 200 mg L^{-1}; (2)88 ~ 122 d, SO_4^{2-}: 250 mg L^{-1} (L1), 230 mg L^{-1} (L2); (3) 124 ~ 174 d, SO_4^{2-}: 300 mg L^{-1} (L1), 250 mg L^{-1} (L2)

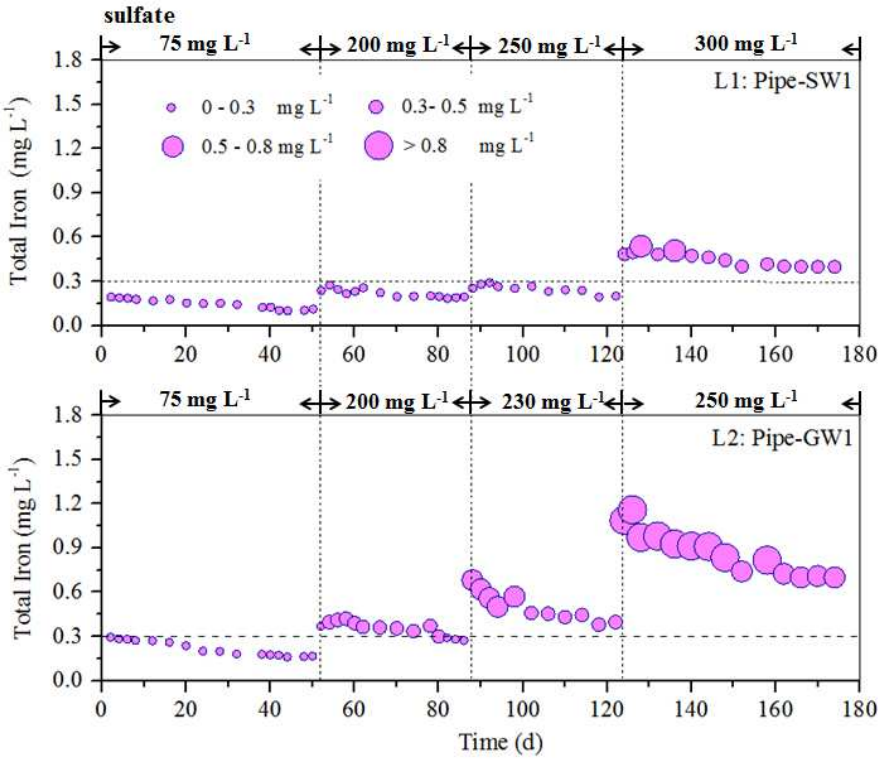

Fig. 2 Total iron release of L1 and L2 under different sulfate concentrations

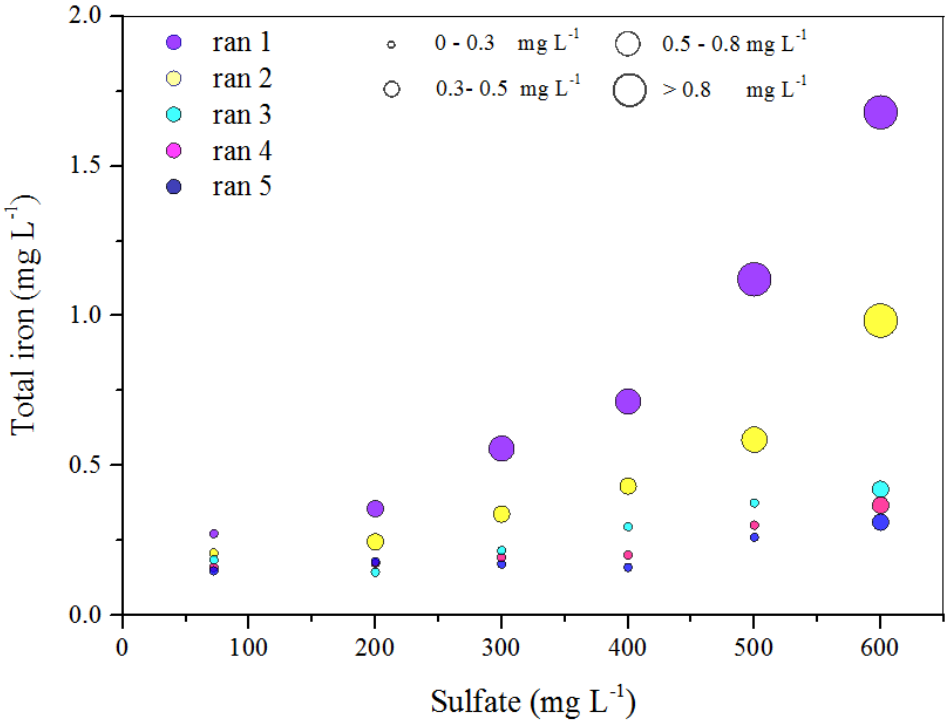

Fig. 3 Total iron release of L3 under different sulfate concentrations

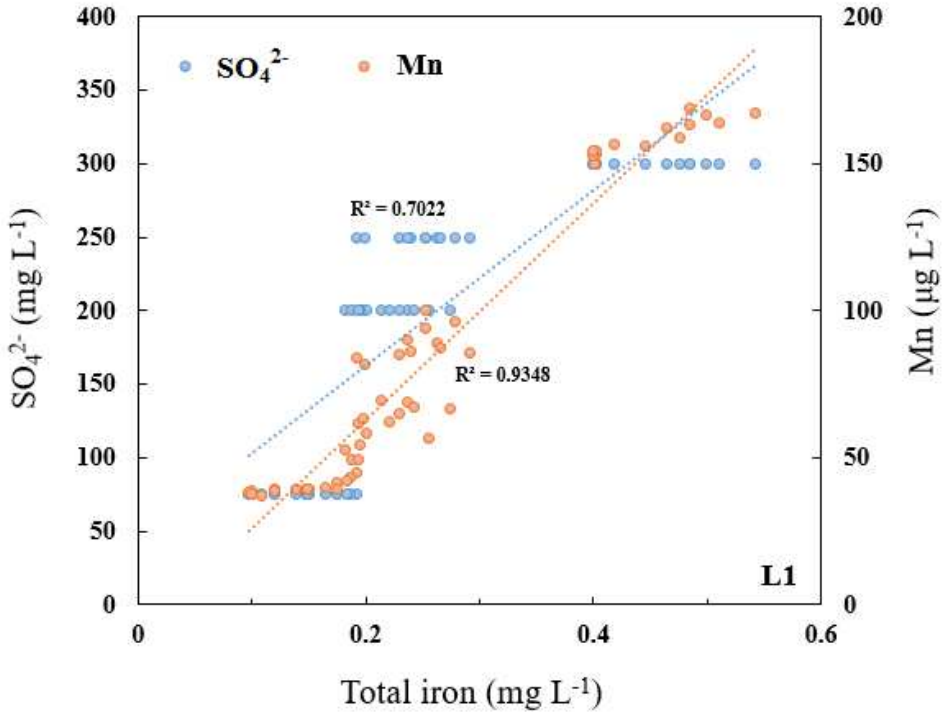
SO4 2-
Mn
R² = 0.7022
R² = 0.9348
L1
SO4 2- (mg L-1)
Mn (µg L-1)
Total iron (mg L-1)
0
50
100
150
200
250
300
350
400
0
0.2
0.4
0.6

(a)

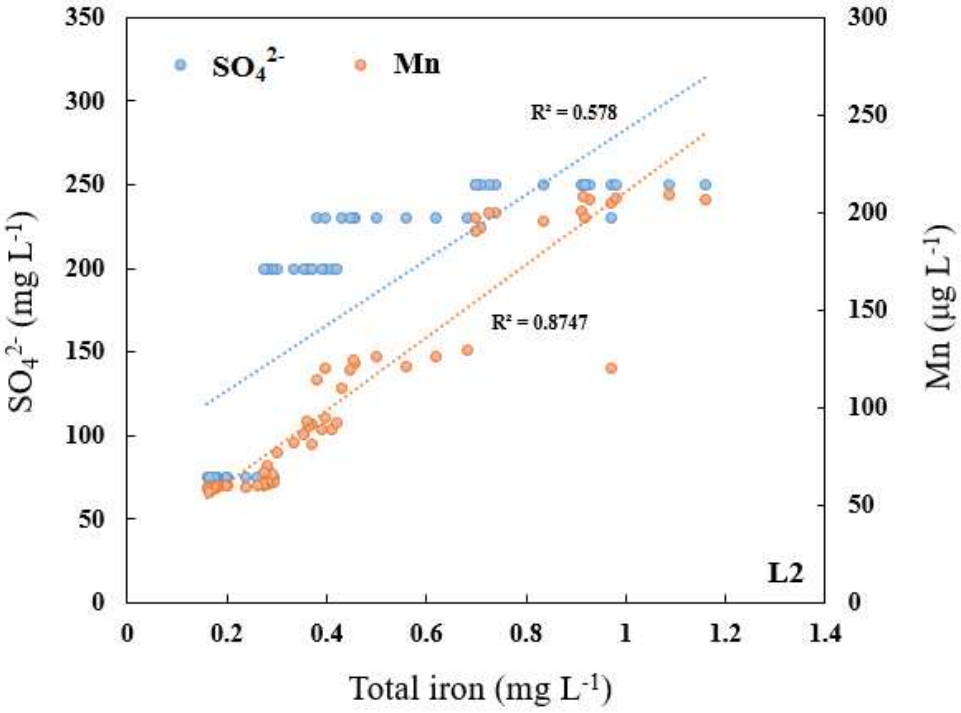
SO4 2-
Mn
R² = 0.578
R² = 0.8747
L2
SO4 2- (mg L-1)
Mn (µg L-1)
Total iron (mg L-1)
0
50
100
150
200
250
300
350
0
0.2
0.4
0.6
0.8
1
1.2
1.4

(b)

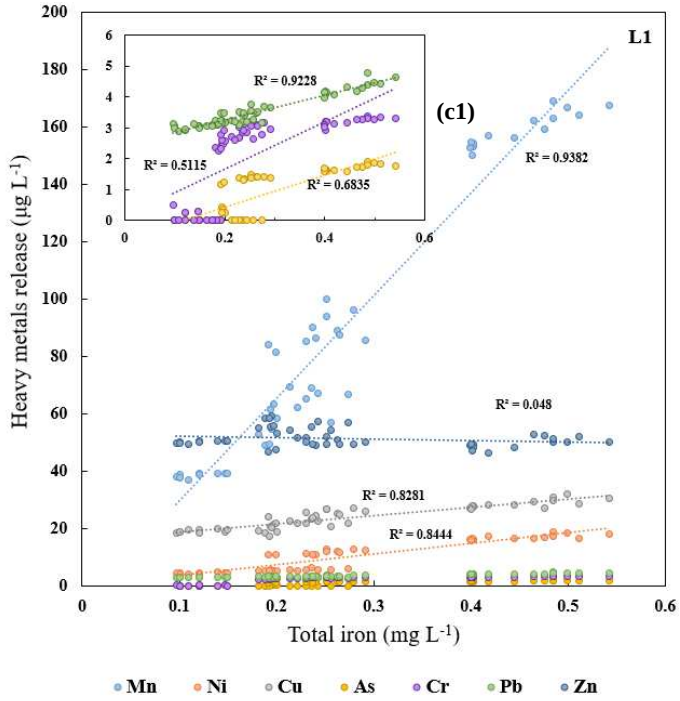

(c)

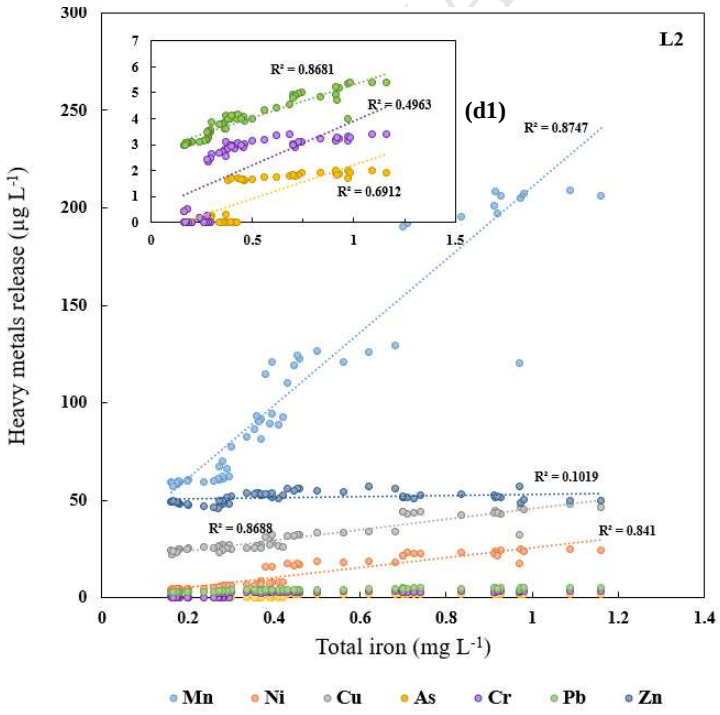

(d)

Fig. 4 Relationships between the concentrations of total iron & sulfate/Mn (a: L1, b: L2) and total iron & heavy metals (c: L1, d: L2)

The small plots (c1, d1) in (c) and (d) are the enlarged views of the relationships between the concentrations of Fe & As, Fe & Cr and Fe & Pb.

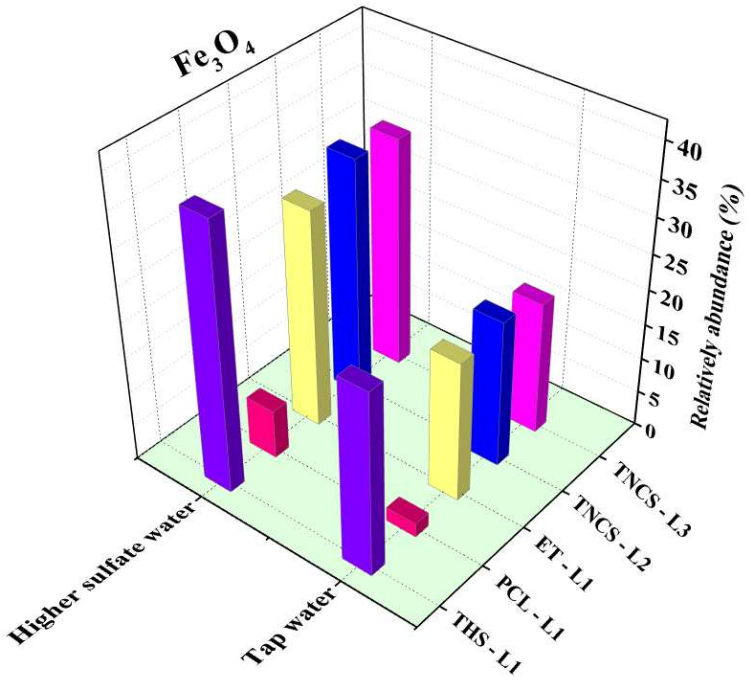
Fe3O4
Relatively abundance (%)
0
5
10
15
20
25
30
35
40
Higher sulfate water
Tap water
THS - L1
PCL - L1
ET - L1
TNCS - L2
TNCS - L3

(a)

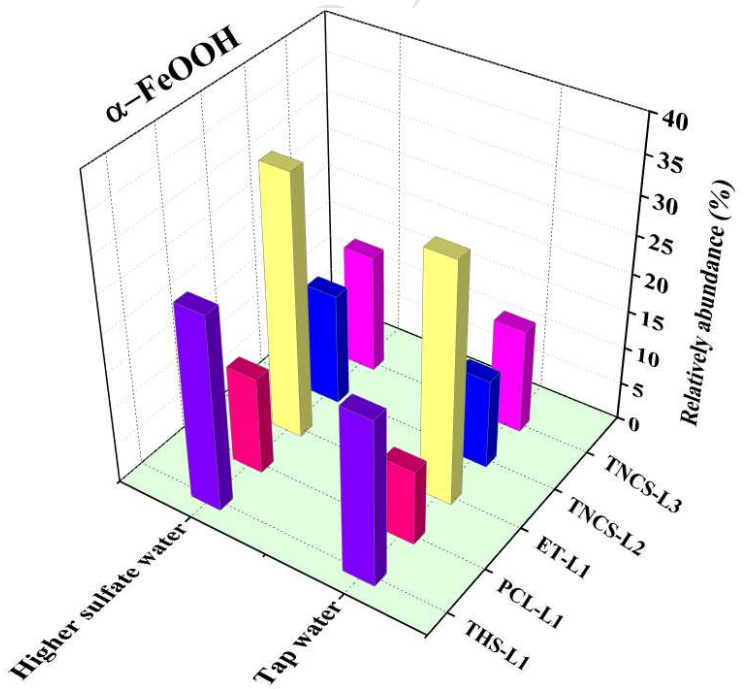
α–FeOOH
Relatively abundance (%)
0
5
10
15
20
25
30
35
40
Higher sulfate water
Tap water
THS-L1
PCL-L1
ET-L1
TNCS-L2
TNCS-L3

(b)

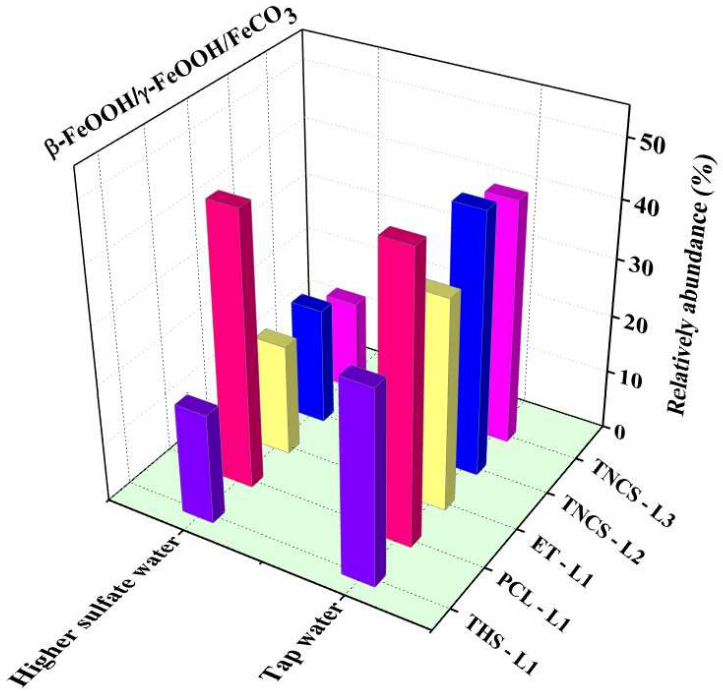
β-FeOOH/γ-FeOOH/FeCO3
Relatively abundance (%)
0
10
20
30
40
50
Higher sulfate water
Tap water
THS - L1
PCL - L1
ET - L1
TNCS - L2
TNCS - L3

(c)

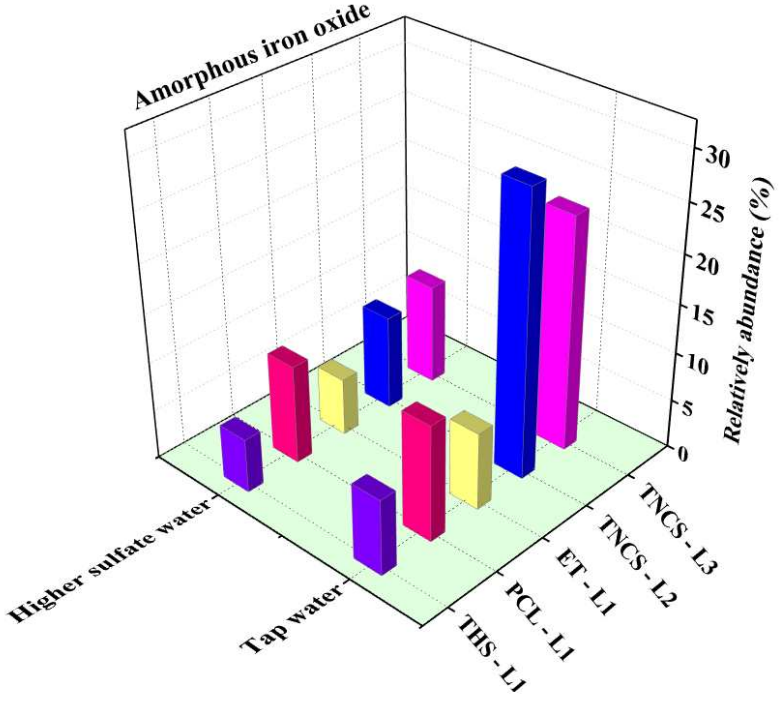
Amorphous iron oxide
Relatively abundance (%)
0
5
10
15
20
25
30
Higher sulfate water
Tap water
THS - L1
PCL - L1
ET - L1
TNCS - L2
TNCS - L3

(d)

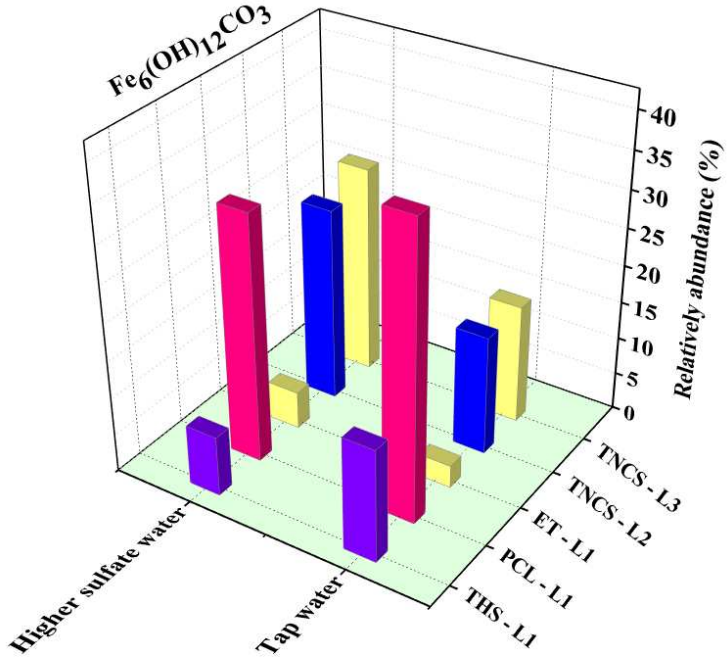

(e)

Fig. 5 Crystalline composition variation of THS, PCL, ET and TNCS combined samples for pipe loops L1-L3 under different experimental conditions
(a) Fe_3O_4, (b) α-FeOOH, (c) β-FeOOH / γ-FeOOH / $FeCO_3$, (d) Amorphous iron oxide, (e) $Fe_6(OH)_{12}CO_3$,

Highlights

- Sulfate could trigger heavy metal release from iron corrosion scales.
- Strong correlations exist between the releases of total iron and heavy metals.
- Heavy metals release decrease slowly over time after sudden increase by sulfate.
- Corrosion scale stabilization and SRB growth inhibit heavy metals release.